

PAPER View Article Online



Cite this: Phys. Chem. Chem. Phys., 2017, 19, 29134

Received 11th August 2017, Accepted 14th October 2017

DOI: 10.1039/c7cp05489k

rsc.li/pccp

Influence of molecular weight on ion-transport properties of polymeric ionic liquids†

We report the results of atomistic molecular dynamics simulations on polymerized 1-butyl-3-vinylimidazolium-hexafluorophosphate ionic liquids, studying the influence of the polymer molecular weight on the ion mobilities and the mechanisms underlying ion transport, including ion-association dynamics, ion hopping, and ion-polymer coordinations. With an increase in polymer molecular weight, the diffusivity of the hexafluorophosphate (PF $_6$ -) counterion decreases and plateaus above seven repeat units. The diffusivity is seen to correlate well with the ion-association structural relaxation time for pure ionic liquids, but becomes more correlated with ion-association lifetimes for larger molecular weight polymers. By analyzing the diffusivity of ions based on coordination structure, we unearth a transport mechanism in which the PF $_6$ - moves by "climbing the ladder" while associated with four polymeric cations from two different polymers.

1 Introduction

Polymeric ionic liquids (polyILs) have been explored as new materials for versatile solid polymer electrolytes since the pioneering experiments of Ohno and Ito.^{1–5} Although experimental results have shown that polyILs exhibit lower conductivity compared to their nonpolymeric counterparts,^{6–10} research has persisted due to the promise of improved mechanical stability^{11–14} and reduced charge polarization^{15–23} for battery electrolyte applications.^{8,24–31}

Ion motion in conventional salt-doped polymer electrolytes, such as polyethylene oxide (PEO) and other materials, is strongly slaved to the polymer segmental relaxation dynamics. $^{32-38}$ Such a coupling between the conductivity and the mechanical properties has proven to be a significant hurdle for the optimization and design of mechanically strong but highly conducting polymer electrolytes. In recent experiments of Sokolov, Sangoro and coworkers, $^{39-41}$ the coupling between the structural relaxation time and ionic conductivity was found to be similarly applicable for pure ILs. However, for polyILs, a decoupling, manifesting as a "superionic" dependence of the conductivity on the structural relaxation times was observed. $^{42-44}$ Explicitly, Fan *et al.* demonstrated that long polyILs have a higher conductivity than short polyILs and pure ILs when compared at the same glass-transition-normalized temperature (T/T_g). 44 Such experimental results have raised interest

Motivated by the above issues, in a recent communication, ⁴⁵ we reported the results of atomistic molecular dynamics simulations on the mechanisms underlying ion motion and diffusivities in a specific model system of poly(1-butyl-3-vinylimidazolium-hexafluorophosphate) (pBVIm⁺-PF₆⁻) polyIL electrolytes containing 32 repeat units. There we demonstrated that anion transport in polyILs occurs through a mechanism involving intra- and intermolecular ion hopping through the formation and breaking of ion associations involving four polymerized cationic monomers bonded to two different polymer chains. The resulting ion mobilities were shown to be directly correlated with the average lifetimes of ion associations. Moreover, such a trend was demonstrated to contrast with the behavior in pure ILs, wherein ionic motion is more closely correlated with structural relaxations of the surrounding medium.

In the present work, we expand upon the results of our earlier brief communication⁴⁵ by characterizing the ion transport properties of pBVIm⁺-PF₆⁻ polyILs of varying number of repeat units ranging from pureILs to longer chain polyILs (Fig. 1). Consistent with corresponding experimental results, our simulations indicate that the ionic diffusivity decreases with increasing molecular weight and plateaus to an almost constant value for longer polymers. At the same time, ion motion is seen to become less correlated with structural

in polyILs as potential candidate materials to overcome the tradeoff between mechanical strength and conductivity that plagues many polymer electrolytes. In turn, such observations have also raised fundamental questions on the mechanisms and time scales underlying ion-transport in polyILs, and the origin of differences in ion transport phenomena within polyILs and pure ionic liquids.

^a Department of Chemical Engineering, The University of Texas at Austin, Austin, TX, USA. E-mail: venkat@che.utexas.edu; Fax: +1-512-471-7060; Tel: +1-512-471-4856

b Department of Chemical and Biomolecular Engineering, University of Illinois at Urbana-Champaign, Champaign, IL, USA

 $[\]dagger$ Electronic supplementary information (ESI) available: Additional data supporting our methods and conclusions. See DOI: 10.1039/c7cp05489k

Paper PCCP

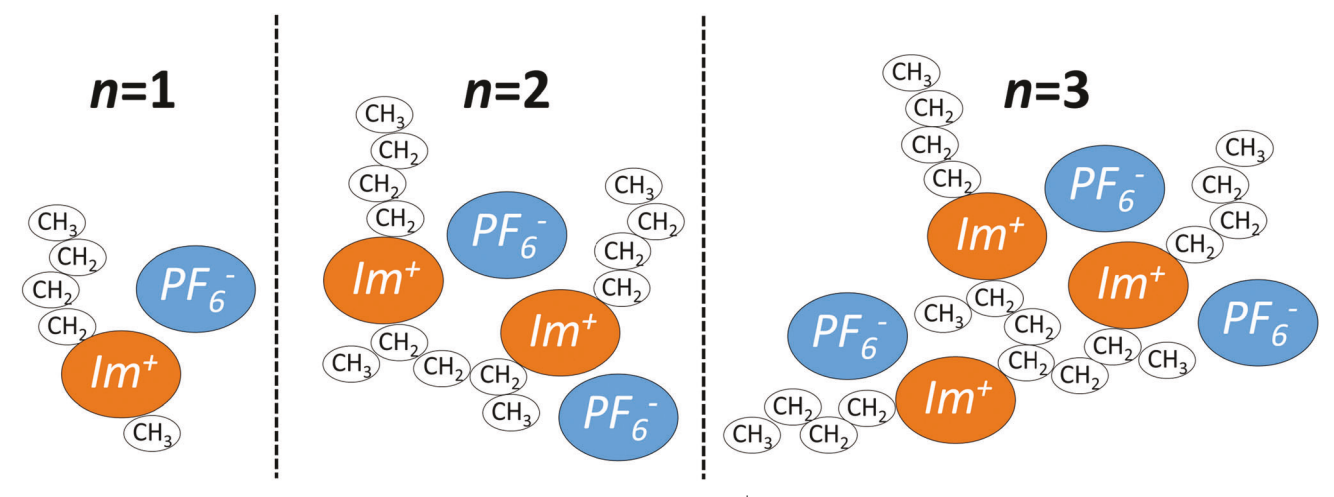


Fig. 1 Chemical composition of molecules corresponding to n=1, 2, and 3, where Im⁺ consists of three carbon (and hydrogen) and two nitrogen atoms in a resonance-stabilized ring. The carbon chains (butyl fragment and polyethylene backbone) are bonded to different nitrogen atoms. Note that n=1 corresponds to a pure IL, 1-butyl-3-methylimidazolium(BMIm)-PF₆⁻ (see n=1 in figure), which was investigated in depth in our earlier study.⁴⁵ Polymers investigated in the present study contain n butyl-imidazolium units bonded to alternating carbon atoms of a methyl-capped-polyethylene backbone, as shown for n=2 and 3.

relaxation times and more correlated with ion-association lifetimes. Additionally, we characterize ionic and polymer coordination and show that the ions move by a motion which resembles climbing a ladder with four polymeric cations from two different polymers.

2 Methods

2.1 Interaction potentials

A number of earlier studies have investigated pure ILs using molecular-dynamics (MD) simulations^{46–50} and multiscale coarse-graining (CG).^{51,52} In this work, we used all-atom MD simulations to pursue the objectives detailed in the introduction. Explicitly, MD simulations in this work utilized the following interaction potential:

$$\begin{split} U &= \sum_{r} U_{\rm bond}(r) + \sum_{\theta} U_{\rm angle}(\theta) + \sum_{\phi} U_{\rm dihedral}(\phi) \\ &+ \sum_{\phi} U_{\rm impropers}(\phi) + \sum_{ij} U_{\rm nb}(r_{ij}). \end{split} \tag{1}$$

The bond and angle interactions are described by harmonic potentials $U_{\text{bond}}(r) = k_r(r - r_0)^2$ and $U_{\text{angle}}(\theta) = k_\theta(\theta - \theta_0)^2$ with spring constants k_r and k_θ , and equilibrium bond length r_0 and angle θ_0 . The energy contribution from dihedral angles is modeled using the OPLS-style dihedral potential in LAMMPS MD software:⁵³

$$U_{\text{dihedral}}(\phi) = \frac{1}{2} \sum_{n=1}^{4} K_n \left[1 + (-1)^{n+1} \cos(n\phi) \right]. \tag{2}$$

The energy contribution of all improper angles in which the centered atom is part of the imidazolium ring is represented by $U_{\rm improper}(\phi)=1.1[1-\cos(2\phi)]$. Finally, non-bonded interactions between particles i and j are modeled with 12-6 Lennard-Jones (LJ) and Coulombic potentials:

$$U_{\rm nb}(r_{ij}) = 4\varepsilon_{ij} \left[\left(\frac{\sigma_{ij}}{r} \right)^{12} - \left(\frac{\sigma_{ij}}{r} \right)^{6} \right] + \frac{Cq_{i}q_{j}}{r}, \tag{3}$$

with potential-well depth ε_{ij} , van der Waals radius σ_{ij} , and charges q_i and q_j in fundamental units of charge (e). The LJ interaction parameters for cross terms were derived using geometric combining rules, $\varepsilon_{ij} = \sqrt{\varepsilon_i \varepsilon_j}$ and $\sigma_{ij} = \sqrt{\sigma_i \sigma_j}$. The energy-conversion constant $C = 5.514 \times 10^{-22}$ kcal Å e⁻² is used to complete the Coulombic potential.

2.2 Development of the force field parameters and partial charges

We adapted most of the intra- and inter-molecular force field parameters from earlier studies. 45,54-56 Specifically, the parameter set originated in Jorgensen's all-atom optimized potential for liquid simulations force field (OPLS-AA).54 Bhargava and Balasubramanian reported improved parameters for 1-butyl-3methylimidazolium(BMIm+)-PF6- to accurately reproduce experimental density and diffusion coefficients.⁵⁶ Sambasivarao et al. contributed further refinements to the intramolecular parameters for BMIm⁺-PF₆⁻, particularly for the energy contribution of dihedral angles.55 We collected and applied these developments in our earlier work for pBVIm⁺-PF₆ with n = 32.45 We derived unscaled partial atomic charges from quantum chemistry calculations using the AMBER antechamber tool. 57,58 The electrostatic distribution was obtained from electronic structure optimization using Gaussian09 with a B3LYP hybrid functional using the 6-311G(d,p) basis set.59

We note that the OPLS-AA force field has been utilized in past studies to accurately model the physical properties of ILs and polymers. ^{55,56,60–62} Such efforts have been mostly successful in matching experimental structural and thermodynamic properties, including density and heats of vaporization. ⁵⁵ However, apart from Bhargava and Balasubramanian, who demonstrated good agreement with experimental diffusion coefficients, ⁵⁶ these studies did not reproduce accurate transport properties. Polarizable force fields have been utilized in some studies to produce accurate transport properties in ILs, ^{63–67} but prove to be computationally

expensive, even for non-polymeric ILs. Others have circumvented the computational expense of such methods by scaling partial atomic charges to study IL systems, ^{47,56,68-74} including the aforementioned work by Bhargava and Balasubramanian. Several studies demonstrated that uniformly scaling partial atomic charges by 0.7–0.9 (depending on IL type) was successful in matching structural and transport properties. ^{56,70,71,73,74} Based upon the efficiency and accuracy of such methods, we have utilized the charge scaling approach with a 0.8 scaling factor, suggested by Bhargava and Balasubramanian. ⁵⁶ Dommert *et al.* provides a review of force fields for modeling both structural and dynamic properties in ILs, ⁶¹ and we refer the interested reader to the discussion within on using charge scaling *versus* polarization to match a wider range of properties.

2.3 Initialization, equilibration, and simulation procedure

Atomistic MD simulations were performed using the LAMMPS software package.⁵³ LJ and Coulombic interactions were evaluated up to a direct-sum cutoff of 10 Å. Beyond this cutoff, we employed tail corrections for the Lennard-Jones interactions and the particleparticle particle-mesh (PPPM) solver with a tolerance of 10⁻⁵ for long-range Coulombic interactions. 75,76 All simulations in the present work were conducted using periodic boundary conditions in the constant pressure and temperature (NPT) ensemble, adjusting the temperature every 0.1 ps and the pressure every 1.0 ps with a Nosé-Hoover thermostat and Parinello-Rahman barostat. 77-80 Forces and positions were evaluated at a regular time step of 2.0 fs. Hydrogen bonds were constrained to their equilibrium length using the SHAKE algorithm.81 Heating and cooling was applied through incremented temperature changes using a Langevin thermostat, 82 with a time step of 1.0 fs for a total of 100 ps (henceforth referenced as the TC simulation).

Polymers with n=2, 3, 5, 7, 8, 9, 10, 11, 12, and 16 were constructed using Gaussview. Identical copies of these molecules were randomly packed using Packmol in a cubic simulation box of length 240 Å containing at least 800 imidazolium(Im⁺)-PF₆⁻ ion pairs. ⁸³ We performed a series of equilibration steps on each system, which are listed below. Temperature, pressure, and the length of the simulation are identified for all *NPT* simulations.

- (1) Heat to 1000 K using TC simulation,
- (2) *NPT* simulation at 1000 K and 0.05 atm for 1 ns with a time step of 0.5 fs; forces evaluated without long-range Coulombic contribution; hydrogen bonds unconstrained,
- (3) *NPT* simulation at 1000 K and 1 atm for 2 ns with a time step of 1.0 fs; forces evaluated without long-range Coulombic contribution; hydrogen bonds unconstrained,
 - (4) cool to 600 K using TC simulation,
- (5) NPT simulation at 600 K and 1 atm for 2 ns with a time step of 1.0 fs; forces evaluated without long-range Coulombic contribution; hydrogen bonds unconstrained,
- (6) NPT simulation at 600 K and 1 atm for 2 ns with a time step of 1.0 fs,
 - (7) NPT simulation at 600 K and 1 atm for 20 ns, and
 - (8) production NPT simulation at 600 K and 1 atm for 50 ns.

The configuration and velocities at the end of the production run served as the starting point for the cooling, equilibration, and production sequence (items 5–8 above) for 575 K, 550 K, 525 K, and 500 K. Pressure, simulation length, and all procedure modifiers were unchanged. In the ESI,† we present evidence of equilibration by displaying the time evolution of potential energy (Fig. S10(a), ESI†), total energy (Fig. S10(b), ESI†) and density (Fig. S11, ESI†).

2.4 Analysis of diffusion coefficients and ion-pair relaxation times

For the purpose of analyzing the dynamics of our systems, all-atom trajectories obtained from MD simulations were coarse-grained to center-of-mass trajectories containing only PF_6^- and Im^+ groups. The entire PF_6^- anion is incorporated into its center-of-mass, while the Im^+ cation contains the eight connected atoms of the imidazolium five-membered ring (three carbon, three hydrogen, two nitrogen). This choice for Im^+ was inspired by the dominant contribution to the cation's positive charge by the imidazolium ring atoms. We calculated the diffusion coeffcients (D) of PF_6^- and Im^+ from the respective mean-squared displacement (MSD) of each center-of-mass by using the Einstein relation,

$$D = \lim_{t \to \infty} \frac{1}{6t} \langle (r(t) - r(0))^2 \rangle, \tag{4}$$

where r(t) denotes the center-of-mass position of ${\rm PF_6}^-$ or ${\rm Im}^+$ at time t. The practical value of the limit is well approximated at a finite time by the slope of the linear portion of the MSD *versus* time plot. We direct the concerned reader to ESI,† Section II.A (Table S7, ESI†), for proof that the diffusivities reported herein are extracted from nearly linear MSD curves. The same section in ESI† addresses other potential concerns regarding the validity of testing "short" timescales for diffusivities. Fig. S3 (ESI†) demonstrates that a short trajectory very slightly overestimates the diffusivity, yet maintains good qualitative agreement with a trajectory of an order of magnitude longer.

To quantify the different time scales underlying ion motion, we identify PF_6^- and Im^+ ions to be associated if their centers of mass are within the first coordination shell (6.5 Å). Alpha In our earlier work, we followed the ideas originally proposed by Chandra and further explored by Zhao *et al.*, and used two distinct population variables to characterize the history of association between ions: (i) h(t) defined such that it takes a value unity if an ion association present at time t = 0 remains intact at time t (albeit, the ions can dissociate and reform in the intervening time interval); and (ii) $H(\tau)$ defined such that it takes a value unity if h(t) is unity for all t from t_0 to $t_0 + \tau$,

$$H(\tau) = \begin{cases} 1, & (h(t) = 1) \forall (t_0 \le t < t_0 + \tau) \\ 0, & \text{otherwise.} \end{cases}$$
 (5)

Based on the above defined functions, h(t) and $H(\tau)$, two distinct timescales were extracted to characterize the dynamics of ion-association relaxations. The first is the timescale associated

with the intermittent time autocorrelation function (ACF) of ion pairs ($C(\tau)$):

$$C(\tau) = \frac{\langle h(t_0)h(t_0 + \tau)\rangle}{\langle h\rangle}.$$
 (6)

By definition, the function $C(\tau)$ captures the relaxation behavior of all possible types of ion associations including isolated ion pairs, multiplets and clusters. The characteristic timescale of relaxation of $C(\tau)$ is obtained by integrating $C(\tau)$ over the positive domain. $C(\tau)$ is well-approximated by a stretched exponential function,

$$C(\tau) = a_0 \exp\left(-\left(\frac{\tau}{a_1}\right)^{a_2}\right),\tag{7}$$

which can be analytically evaluated to obtain the corresponding relaxation time scale, τ_C , as:

$$\tau_{\rm C} = a_0 a_1 \Gamma \left(1 + \frac{1}{a_2} \right). \tag{8}$$

In our earlier work, 45 we also characterized the continuous time ACF $S(\tau)$, defined as

$$S(\tau) = \frac{\langle h(t_0)H(t_0 + \tau)\rangle}{\langle h\rangle}.$$
 (9)

As with $C(\tau)$, $S(\tau)$ can be numerically integrated or analytically evaluated by fitting $S(\tau)$ to the stretched exponential function of eqn (6) to derive the characteristic timescale, τ_S . We chose to analytically integrate $S(\tau)$ to find τ_S . In the present work, we analyzed ionic association from a trajectory saved at every 1 ps when evaluating $C(\tau)$ and $S(\tau)$. This time interval was chosen to optimize the storage resources required and analysis efficiency, and was verified to qualitatively agree with a trajectory of finer saving frequency, as small as 0.01 ps, in our previous report. ⁴⁵

In our earlier study, ⁴⁵ by explicit comparison to decay of the intermediate scattering function S(q,t), we demonstrated that the time scale extracted from the relaxation of ion associations, $\tau_{\rm C}$, corresponds to the true structural relaxation time for

the system. Furthermore, for both pure ILs and polyILs, $\tau_{\rm C}$ was found to follow a nearly universal dependence on the temperature normalized as $T/T_{\rm g}$, where $T_{\rm g}$ corresponds to the glass transition temperature. In contrast, the function $S(\tau)$ represents the probability that a given ion association remains intact from time t_0 to time $t_0+\tau$, and the time scale $\tau_{\rm S}$ extracted from such a function was argued to provide a useful quantification of the average lifetime of the ion associations. Based on such results and other examples in literature, ^{84,86} henceforth we term $\tau_{\rm C}$ as the structural relaxation time and $\tau_{\rm S}$ as the ion-association lifetime.

While the primary objective of the present work is to probe the correlations between the ion diffusivities and different time scales $\tau_{\rm C}$ and $\tau_{\rm S}$, experimentally it has been more common to probe such dependencies (especially relating to the structural relaxation times) in terms of the glass-transition temperature $(T_{\rm g})$ of the system. In our earlier work, ⁴⁵ we extracted the $T_{\rm g}$ s of a pureIL and a polyIL of 32 units using the temperature dependence of the densities of the system, and demonstrated that the simulation results yielded $T_{\rm g}$ s which were very close to experimental values. In the present work, we adapted a similar "equilibrium" procedure to extract the $T_{\rm g}$ s for polyILs of different lengths. The results, presented in ESI† (Fig. S9), demonstrate that the simulation values agree well with the predictions of the Flory–Fox equation $T_{\rm g}$ 0 in describing the molecular-weight dependence of the glass transition temperature:

$$T_{\rm g}(n) = T_{\rm g,inf} - \frac{K}{n},\tag{10}$$

where $T_{\rm g,inf}$ represents the (hypothetical) $T_{\rm g}$ of an infinitely long polymer and K denotes the constant quantifying the molecular weight dependence. Based on such results, and acknowledging the inherent statistical errors associated with the determination of $T_{\rm g}$ from simulation densities, we opted to instead use the experimental values of $T_{\rm g,inf} = 436$ K reported by Nakamura $et~al.^{45,88}$ and the monomer $T_{\rm g}$ of 196 K reported by Shamim $et~al.^{89}$ in

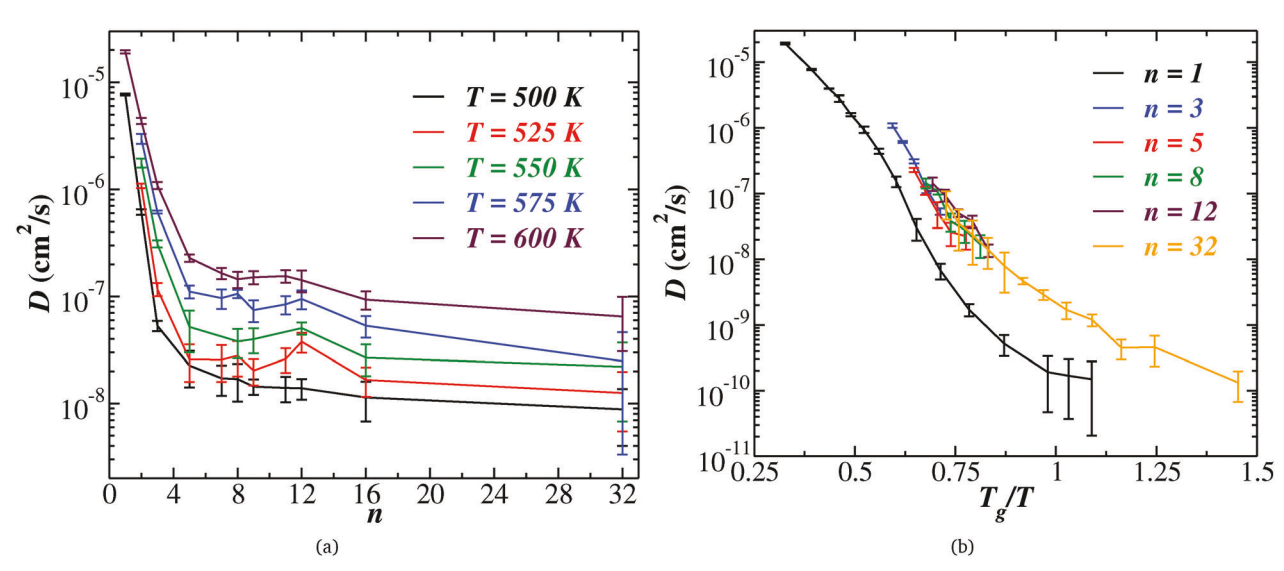


Fig. 2 (a) Diffusivity as a function of the number of repeat units n; and (b) diffusivity of PF_6^- as a function of T_g/T for select cases from this study and ref. 45 (n = 1 and n = 32). Lines are a guide to the eye.

PCCP Paper

conjunction with the Flory-Fox equation to determine the T_g for polyILs of varying length.

3 Results and discussion

3.1 Ion diffusivities

Fig. 2(a) displays the results for PF₆⁻ diffusivity as a function of the number of repeat units, n, for a range of temperatures. It can be seen that the diffusivity drops dramatically when nincreases in the range of two to five monomers. However, the diffusivity changes are seen to become much less significant when n increases from 7 to 32 monomers. These data are qualitatively consistent with the findings of Fan and coworkers, who reported a similar drop in conductivity for polyILs of up to n = 10, whereupon further increase in the molecular weight of the polymer had less impact upon the transport properties.⁴⁴

Since the decoupling of the ion conductivities from the structural relaxation times (and hence, the mechanical properties) is a distinguishing characteristic of polyILs, we base much of our discussion on this phenomena and the underlying mechanisms. A preliminary demonstration of such a decoupling can be established by analyzing the ion diffusitivities as a function of T_g/T , where T_g is the glass transition temperature of the respective material. Both the work by Fan et al.44 and our previous study45 demonstrated that pure ILs have a lower diffusivity than polyILs at equivalent T_{g}/T , which suggests that the polyILs possess higher conductivities for equivalent rheological properties. 44,45 Fig. 2(b) confirms the presence of different behaviors for the diffusivity *versus* T_o/T curves of pure ILs and polyILs, as reported previously in our work⁴⁵ and in that of Fan et al.44 Moreover, consistent with experimental results, we observe that the ion diffusivities are higher for polyILs compared to pure ILs at the same T_g/T . More interestingly, the results displayed in Fig. 2(b) also show that, for the range of n probed in our simulations (n = 2-32), polyILs of different molecular weight do not display significant differences in their dependence on T_{o}/T . However, since T_{o} s in Fig. 2(b) were extracted based on an interpolation of experimental values, we defer further discussion of the decoupling characteristics and their mechanisms to the subsequent sections.

Structural relaxation times

We characterized the structural relaxation times, $\tau_{\rm C}$, as a first step towards probing the mechanisms underlying the decoupling between the ion mobilities and the mechanical properties of polyILs. In Fig. 3 we display the results for $\tau_{\rm C}^{-1}$ as a function of *n* at different temperatures. The general trend of $\tau_{\rm C}^{-1}$ is seen to resemble the behavior of the diffusivity, viz., increasing the temperature is seen to lower the relaxation times, and moreover, in examining the molecular weight dependence of $\tau_{\rm C}$, the most significant changes are seen to occur in the range between two to five repeat units. Further increase in molecular weight is seen to result in a much more gradual increase in $\tau_{\rm C}$.

In Fig. 4, we display the timescale τ_C as a function of normalized temperatures T/T_g . Consistent with the expectations for time scales characterizing structural relaxations, we

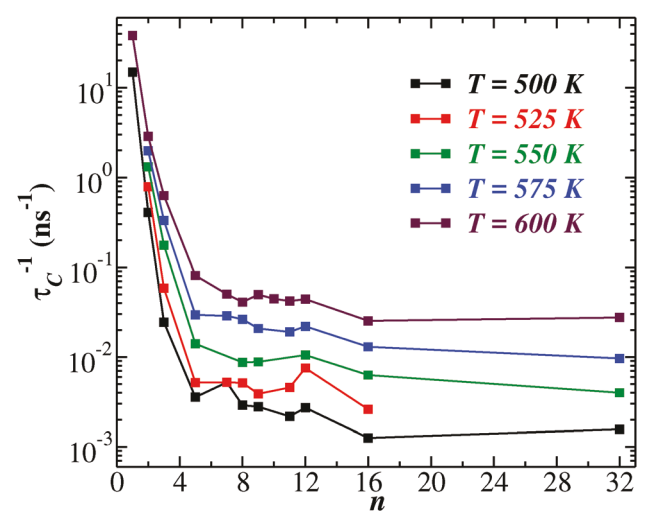


Fig. 3 $\tau_{\rm C}^{-1}$ as a function of n. Data for n=1 and 32 taken from ref. 45.

observe that the $\tau_{\rm C}$ for both polyIL and pure IL systems correlate inversely with T/T_g . Such results confirm that, at the level of structural relaxations, both polyILs and pure ILs exhibit similar characteristics as reflected in their universal dependence of the relaxation times on temperature relative to T_{o} . Such a result also demonstrates that the differences observed in diffusivity from Fig. 2(b) are not a consequence of distinct mechanisms underlying structural relaxations in polyILs and ILs, but rather, a result of different timescales and mechanisms underlying the mobility of ions in polyILs and ILs.

In Fig. 5(a), we display the ionic diffusivities D for different polyILs explicitly as a function of the $\tau_{\rm C}^{-1}$. Shown alongside our results are the experimental results, presented in a similar depiction by Fan et al.44 It can be seen that there is an excellent correlation between the experimental observations and our simulation results. Specifically, the ionic mobilities in ILs are seen to exhibit an "ionic" behavior wherein $D \propto \tau_{\rm C}^{-1}$ (such a result was also demonstrated more exhaustively in simulations

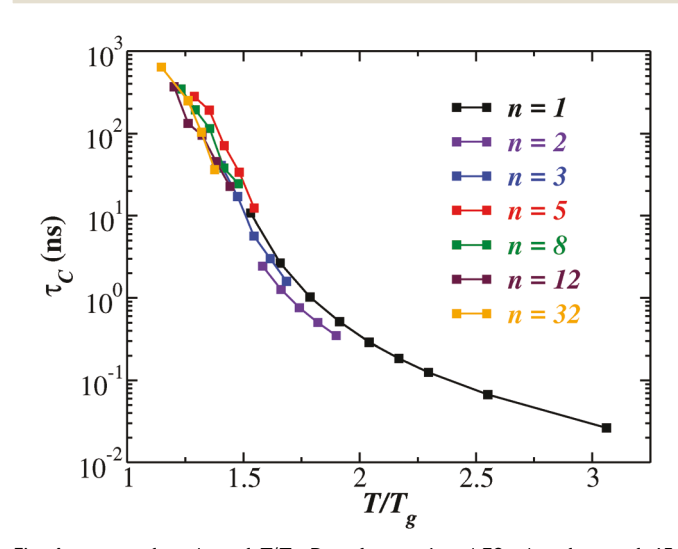


Fig. 4 $\tau_{\rm C}$ as a function of $T/T_{\rm q}$. Data for n=1 and 32 taken from ref. 45.



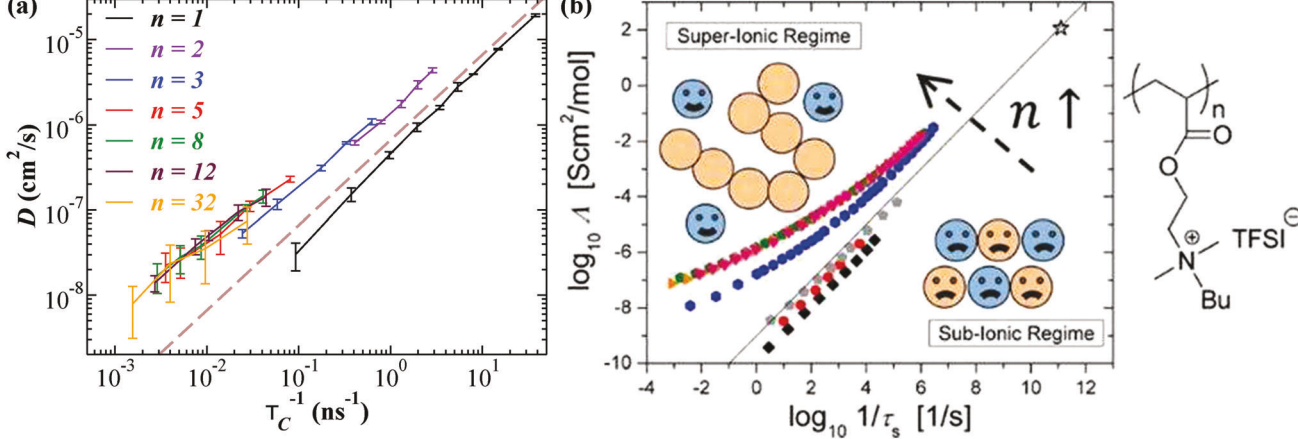


Fig. 5 (a) D as a function of τ_C^{-1} , demonstrating the "super-ionic" behavior of polylLs (D $\propto \tau_C^{-\alpha}$ with $\alpha < 1$) compared to "ionic" behavior exhibited by pure ILs ($D \propto \tau_C^{-1}$); dotted line with slope = 1 to guide the eye. (b) Fan et al. presentation of molar conductivity (A) versus structural relaxation rate (τ_S^{-1}). Reproduced from ref. 44 with permission from ACS.

by Zhang and Maginn by considering a variety of pure ionic liquids⁴¹). In contrast, the polyILs are seen to exhibit a "superionic" behavior $D \propto \tau_{\rm C}^{-\alpha}$, in which $\alpha < 1$. While not readily apparent from the data points themselves, the exponents underlying the fit for polyILs were seen to transition from $\alpha \simeq 0.93$ for short polyILs (n = 2) to $\alpha \simeq 0.75$ for longer polyILs (n = 16, 32), suggesting that there is a gradual transition from the "ionic" behavior to "super-ionic" behavior with an increase in the molecular weight.

Overall, the above results confirm that the ionic mobilities of polyILs are indeed "decoupled" from the structural relaxation times in such systems. Such a decoupling is seen to manifest as a gradual transition from an "ionic" behavior of $D \propto \tau_{\rm C}^{-1}$ for n=1to a "super-ionic" behavior of $D \propto \tau_{\rm C}^{-\alpha}$ ($\alpha < 1$), for n > 1. However, for n > 5, the dependence of diffusivity on structural relaxation times is seen to approach almost universal behavior-a feature also consistent with the experimental observations (Fig. 5(b)).44

Mechanisms underlying ion motion

In the preceding section, we presented results examining the correlation between diffusivity and structural relaxation times, and demonstrated a "decoupling" similar to that observed in experiments. In this section, we seek to identify the mechanisms underlying such a decoupling by characterizing different aspects of ion coordination and motion as a function of molecular weight in polyILs.

A number of prior studies of salt-doped polymer electrolytes, such as PEO, have concluded that ion diffusion in such systems occurs primarily through ion hopping along the polymer backbone. 32-34,37,38 In our earlier work, 45 we presented results which suggested the existence of a similar mechanism in polyILs, but with ion coordination characteristics reflecting electrostatics and chemical interactions specific to polyILs. Explicitly, for n = 32, we demonstrated that ion diffusion manifests from a hopping mechanism, with the most probable coordination state of PF₆⁻ involving four associated Im⁺ from

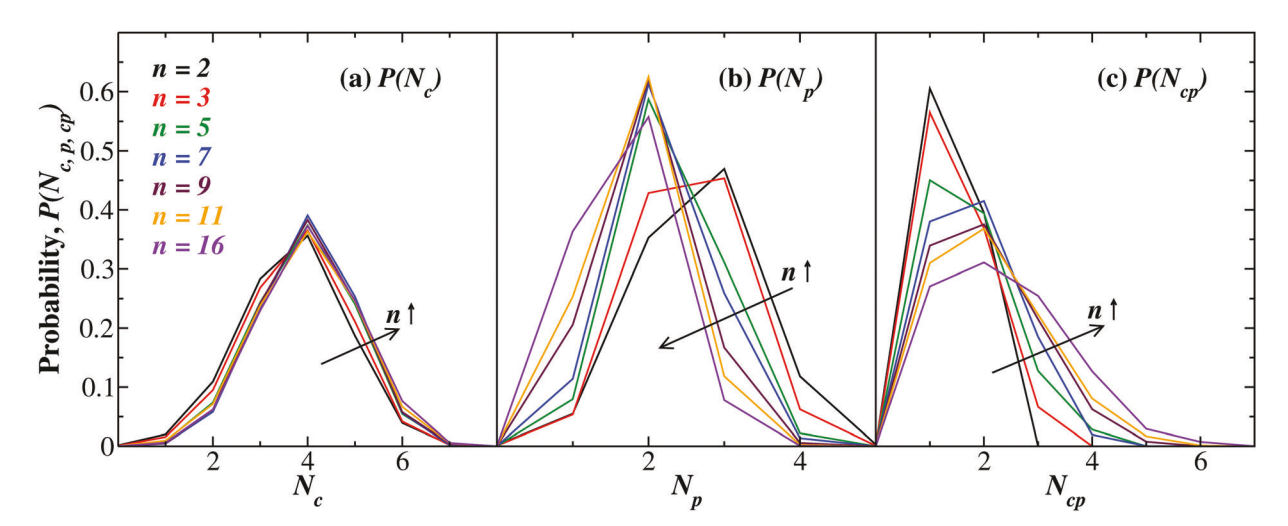


Fig. 6 Probability distribution of coordination states for all hopping events.

two distinct polymers. 45 For the present study, we analyzed the coordination states of PF₆⁻ ions with Im⁺ as a function of molecular weight to compare directly to these results, and also to understand the relationship between these configurations and the dynamics of ion hopping for varying polymer lengths.

In analyzing coordination states, we employed three key metrics: ionic, inter-polymeric, and intra-polymer ionic coordination. Ionic coordination number (N_c) identifies the number of Im^+ within a 6.5 Å cutoff of a given PF₆. For example, Fig. 7 shows a PF₆ with five associated Im^+ , giving $N_c = 5$. Inter-polymeric coordination number (N_p) refers to the number of polymer chains containing Im⁺ within this same cutoff radius. In Fig. 7 PF₆⁻ is associated with polymers 1, 2, and 3, leading to $N_p = 3$. Finally, intra-polymer ionic coordination number (N_{cp}) refers to the number of Im⁺ within the same polymer that are coordinated with a given PF₆⁻. For example, Fig. 7 shows polymer 1 with three Im⁺ monomers associated with the PF_6^- , making $N_{cp(1)} = 3$.

Fig. 6 displays the results for the probability distribution of configuration states for N_c , N_p , and N_{cp} associations. In Fig. 6(a), the peak in the N_c distribution is seen to occur at $N_c = 4$, matching the results presented in Mogurampelly et al. for polyIL of 32 repeat units. 45 More interestingly, this result is seen to be invariant among different polymer lengths, suggesting that the high probability of coordination between an anion and four cations likely represents an inherent coordination feature of the anion and cation of the ILs considered in this work.

Fig. 6(b) displays the distribution of the number of distinct polymers, $N_{\rm p}$, involved in the coordination between an anion and cations. From the peaks in the distributions, it can be deduced that the coordination state of anions involve a larger number of polymers for smaller molecular weight (n) polyILs. In contrast, for larger molecular weight (n) systems, the most probable coordination state (the peak in the N_p distribution) shifts to $N_p = 2$, and becomes invariant with the molecular

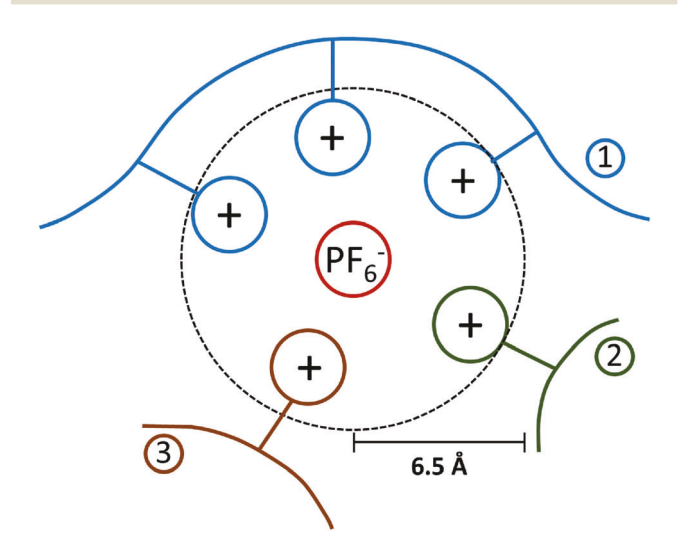


Fig. 7 Schematic representation of coordination state consisting of ionic coordination number N_c = 5; inter-polymeric coordination number N_p = 3; and intra-polymer ionic coordination number $N_{cp(1)} = 3$, $N_{cp(2)} = 1$, $N_{cp(3)} = 1$ 1. Refer to text for definitions of N_c , N_p , and N_{cp} .

weight of the polyILs for $n \geq 5$. Complementing such results, in Fig. 6(c), we quantify the distribution of $N_{\rm cp}$, representing the number of ionic associations with the same polymer molecule. For polyILs of seven or more repeat units, the peak of this distribution is seen to occur at $N_{\rm cp} = 2$.

The discussion presented above relies primarily on the peak values of the equilibrium distributions and does not provide any insights into the influence of such coordination states on the ion mobilities. Moreover, it can be seen from Fig. 6 that significant contributions also arise from other coordination states, such as $N_c = 3$, 5, $N_p = 1$ (particularly for long polyILs), $N_{\rm cp}$ = 1, 3 etc. A true understanding of the impact of such states on ion mobility requires a more detailed characterization of the diffusivity of ions with varying degrees of coordination. Since bulk diffussion occurs on a longer timescale than that which is characteristic of ionic association and dissociation, we could not effectively analyze the direct influence of discrete association states upon the ionic diffusivity. As an alternative, the coordination states $(N_c, N_p, \text{ and } N_{cp})$ for each PF_6 were averaged over the entire simulation and PF₆⁻ with similar values were binned. We then computed the diffusivity of each group of PF₆ using the MSD for the corresponding bin. A more detailed discussion of this method and can be found in Section II.B of ESI.†

Fig. 9 presents the diffusivity of ions grouped within ranges of average N_c , N_p , and N_{cp} values. Overall, diffusivity is seen to be higher when PF₆⁻ is associated with an optimal average ionic configuration between three and four Im⁺. Similarly, for longer polyILs, ions coordinated with $N_{\rm p} \simeq 2$ and $N_{\rm cp} \simeq 2$ are seen to possess generally higher diffusivity. Taken together, the results of Fig. 6 and 9 demonstrate that, for longer polyILs, the state of $N_c = 4$, $N_p = 2$, and $N_{cp} = 2$ is the most likely to occur, while also being the most effective for facilitating ion motion. For smaller polyILs, the peaks in the distribution of N_{cp} are seen occur at smaller values, representative of the smaller number cationic groups available for intramolecular coordination.

As a final step in resolving the mechanisms underlying ion motion in polyILs, we quantified the different kinds of hopping motion underlying ion transport. In our earlier studies, 45,90 dynamical changes in the coordination states of ions were used as a means to identify the ion transport mechanisms in pureILs and polyILs. We continue such a line of investigation in this work, adopting the same definition of such an event, viz., the association or dissociation of a pair of PF₆⁻ and Im⁺ ions over a time interval of 1 ps. 45 Our subsequent study updated the two categories of hopping events, intra- and intermolecular, based on the static coordination state of the PF₆⁻ ion in the dissociated frame. 90 In an intramolecular hopping event (type 1), PF₆ ions move from monomer to monomer along the same polymer. To define this precisely, during the association or dissociation of a given PF₆⁻-Im⁺ pair, if one or more Im⁺ from the same polymer as the participating Im⁺ are associated with the PF₆ when the pair is dissociated, then the event is type 1. In contrast, for intermolecular hopping events (type 2), PF₆ hopping occurs between different polymers. Again, to define this precisely, given an association or dissociation event involving a

PCCP Paper

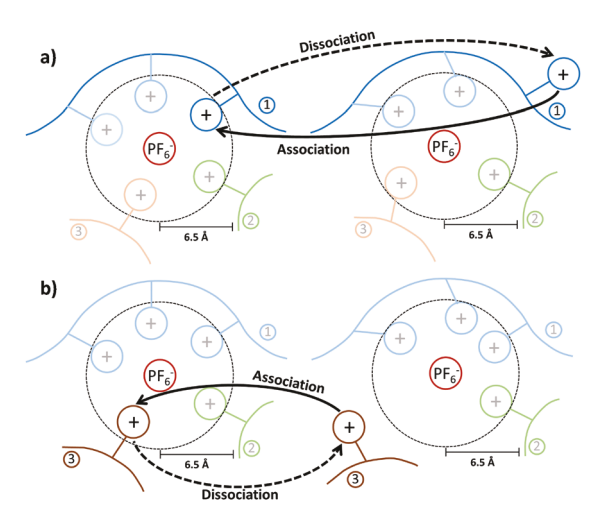


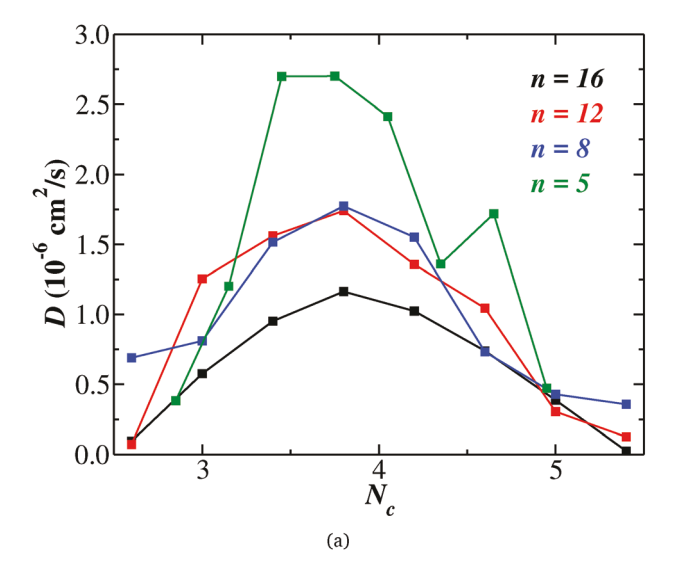
Fig. 8 Diagrams depicting an example (a) intramolecular (type 1) and (b) intermolecular (type 2) hopping event.

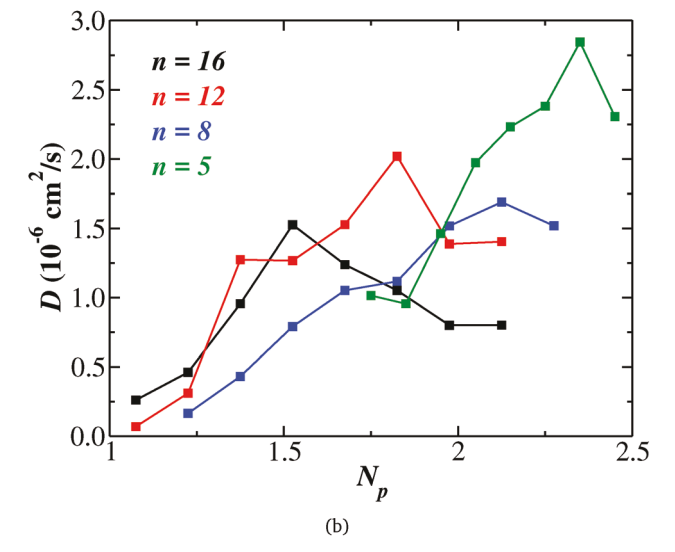
PF₆⁻-Im⁺ pair, if no other Im⁺ from the same chain are associated with the PF₆⁻ when the pair is dissociated, then the event is type 2.

Fig. 8, borrowed from the ESI† of our previous work, 90 illustrates both categories of hopping events. 90 These diagrams do not exhaustively define type 1 or type 2 events, but serve to illustrate the definitions. In Fig. 8(a), polymer 1 in the left frame has three Im⁺ associated with the PF₆⁻ ion, evolving to a state in the right frame with two associated Im⁺. As indicated by the dotted arrow, this is a type 1 dissociation event. The reverse, indicated by the solid arrow, is a type 1 association event. For both cases, in the frame where the ion pair in question is dissociated (right), at least one other Im⁺ from the same chain is associated, indicating that the event is type 1. Fig. 8(b) shows polymer 3 in the left frame with one Im⁺ associated with the PF₆⁻ ion, evolving to a state in the right frame where it has no Im⁺ associated with the given PF₆⁻. The dotted line represents a type 2 dissociation event, while the solid line depicts a type 2 association event. As in the previously example, and by definition, these are type 2 events because polymer 3 is completely unassociated with the PF₆⁻ ion when the PF₆⁻ and Im⁺ pair undergoing the event are unassociated.

In Fig. 10, we present results depicting the molecular weight and temperature dependence of the frequency of type 1 (Fig. 10(a)) and type 2 (Fig. 10(b)) events quantified from the hopping analysis described above. In line with intuitive expectations, the frequency of hopping events is seen to increase with increasing temperature. More pertinent to the subject of this article, Fig. 10(a) and (b) demonstrate that with increasing polymer molecular weight, the frequency of type 1 hopping events generally increases, whereas, the frequency of type 2 hopping events decrease.

Taken together, the results of Fig. 6, 9 and 10 provide a molecular picture of ion motion in ILs and polyILs, along with the explicit differences in the mechanisms underlying the different systems. Specifically, ion motion in polyILs is seen to involve a coordination state of four Im⁺ from two different





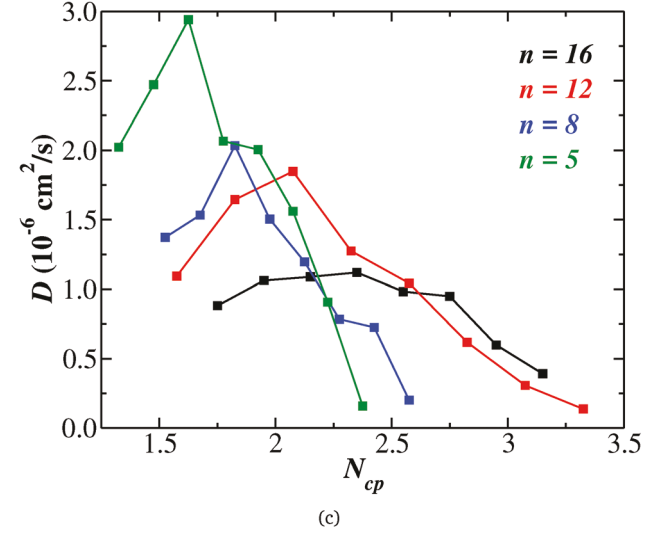


Fig. 9 Diffusivity of PF_6^- binned by (a) average N_c , (b) average N_p , and (c) average N_{cp} for polymer systems of five or more monomers.

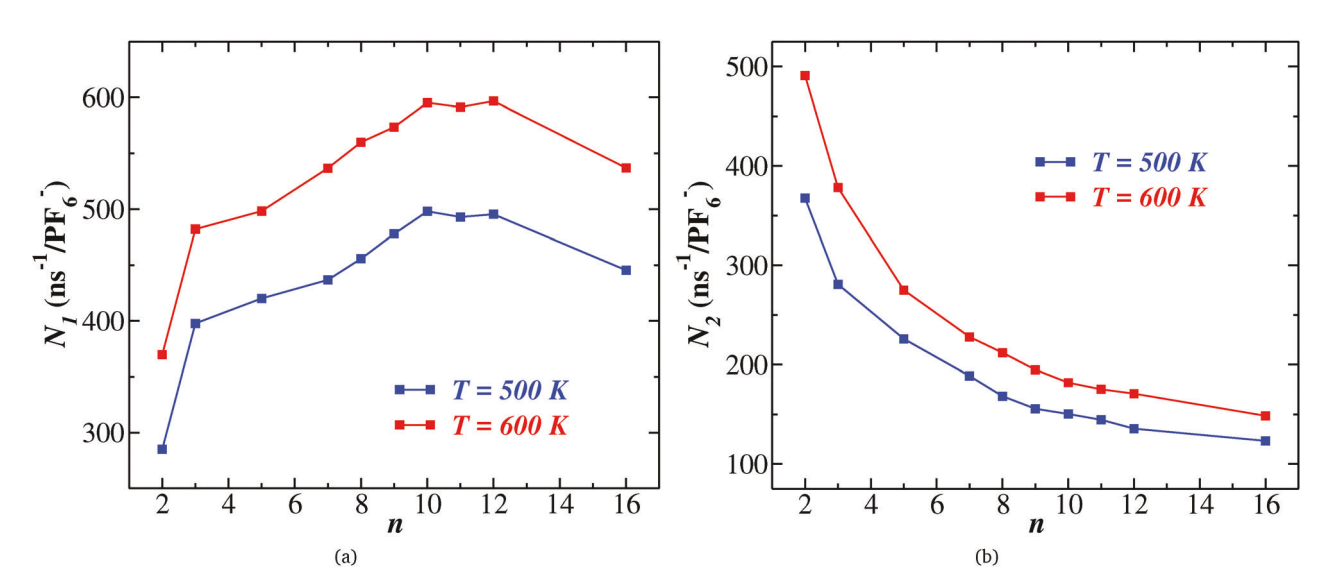


Fig. 10 Frequency of (a) type 1 and (b) type 2 hopping events as a function of n

polymers, with two Im⁺ belonging to each participating polymer. For smaller polyILs, more variability is seen in the polymer coordination numbers, likely influenced by the more limited possibility for intramolecular coordination in addition to the lower densities (and higher free volumes in smaller linker systems). Complementary dynamic analysis demonstrated that ion motion in ILs and small molecule polyILs involve mostly intermolecular hopping between distinct polymers. In contrast, in high molecular weight polyILs, ion motion primarily involves intramolecular hopping, which preserves the identities of the associated polymers. The latter is akin to an ion motion which "climbs the ladder" between two polymer molecules *via* type 1 hopping along two associated polymers.

The above observations provide insights regarding the origin of decoupling between mobilities and structural relaxations observed in large MW polyILs. Explicitly, the observation that intermolecular hopping involving multiple polymer chains underlies ion motion

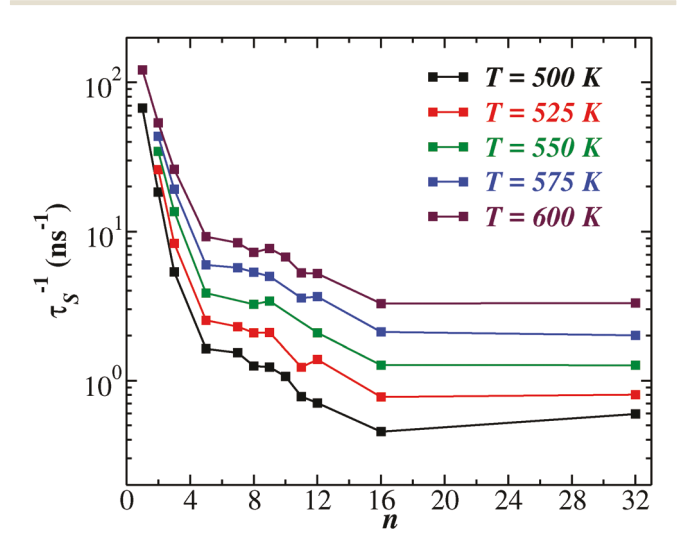


Fig. 11 τ_S as a function of n.

in small molecule polyILs is consistent with the structural relaxation dynamics of the medium, *i.e.* of the polymer chains surrounding the associated ions, being of importance for such system. ^{41,44} In contrast, for long molecule polyILs, intramolecular hopping involving identical polymer chains were seen to play a role. For such motion, it can be envisioned that the structural relaxations of the surrounding medium are less important in influencing the ion motion.

For ion transport dominated by intramolecular hopping, the ion mobilities can be expected to be correlated more strongly to the average lifetimes of anion–cation associations instead of the structural relaxation times in such systems. Indeed, in our earlier work, for polyILs of n=32 it was demonstrated that average ion-association lifetimes, $\tau_{\rm S}$, provides a better characterization of the timescales underlying ionic mobilities in polyILs. More explicitly, it was shown that the $D \propto \tau_{\rm S}^{-1}$ (for n=32) over the entire range of temperatures investigated therein. Below, we present the dependence of the average ion-association lifetimes on the molecular weights (and temperature) to explicitly probe the transition of this correlation from short to long polyILs.

In Fig. 11, we display the results for τ_S as a function of n. Broadly, the trends for τ_S are seen to resemble the behaviors observed in the context of ionic diffusivity and the structural relaxation time (τ_C). Specifically, in increasing the molecular weight, the most significant changes in τ_S are seen to occur in the range between one to five repeat units, and further increase in molecular weight is seen to result in a much a more gradual increase in τ_S . Such results are not surprising, since systems in which the matrix (either ILs or polyILs) exhibits faster dynamics are expected to facilitate more dissociation events.

In Fig. 12, we depict a quantitative comparison of the correlation between the diffusivities and average ion-association lifetimes, $\tau_{\rm S}$. Within the representation of $D \propto \tau_{\rm S}^{-\beta}$ it is seen that the diffusivities indeed transition from $\beta > 1$ for short polyILs to $\beta \simeq 1$ for long polyILs. The non-monotonic trend in exponent

Paper

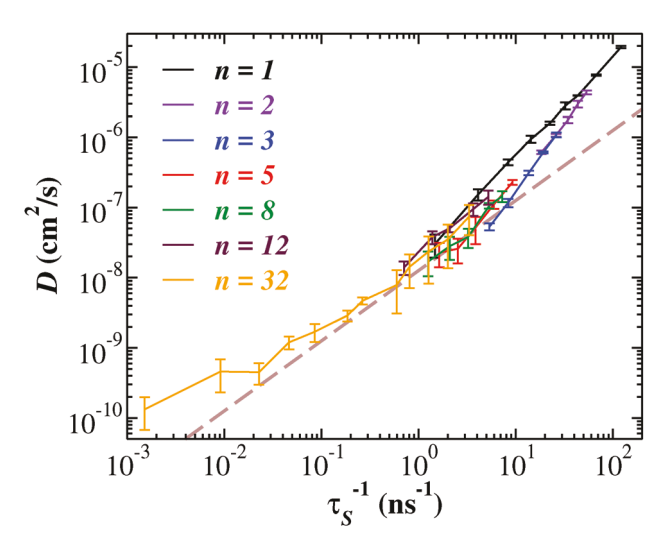


Fig. 12 Diffusivity D as a function of ion-pair lifetime τ_s . Line of slope = 1 to guide the eye

between n = 1 and 3 may be due to a lower rate of back-reactions (reassociations) in pure IL systems compared with short polyIL systems. These results confirm the transition to intramolecular anion hopping as the dominant mode of ion transport in polyIL membranes, and identify the molecular mechanism underlying the decoupling of the ionic mobilities from structural relaxations.

4 Conclusions

We used atomistic molecular dynamics simulations to investigate PF₆ diffusion in poly(1-butyl-3-vinylimidazolium-PF₆) polyILs with varying number of repeat units. Ion diffusivity was observed to decrease with an increase in the molecular weight of the polyILs. For short polyILs, we observed consistency with previously reported linear relationships between diffusivity and structural relaxation time for pure ionic liquids. 39-41,45 For longer polyILs, we observed deviations from such a linear relationship with a behavior mirroring experimental observations.

We explored the nature of ion hopping, and demonstrated that the frequency of intramolecular (type 1) hopping events increases, and the frequency of intermolecular (type 2) hopping events decreases monotonically as the number of repeat units increase. This observation supports the traditional perspective of ion hopping within polymer electrolyte and polyIL systems, which highlights the importance of ion hopping along a polymer backbone in diffusion processes. Analysis of coordination states suggested that the highest mobility ions move via a "ladder mechanism," involving two polymers, each with one, two, or three Im⁺ ions associating with a given PF₆⁻. In support of such a mechanism, the ion diffusivity was seen to transition to an inverse correlation with the average lifetime of ion pairs as the number of repeat units increases.⁴⁵

Conflicts of interest

There are no conflicts to declare.

Acknowledgements

The authors acknowledge the Texas Advanced Computing Center (TACC) at The University of Texas at Austin for providing computing resources that have contributed to the research results reported within this paper. We acknowledge funding in part by grants from the Robert A. Welch Foundation (Grant F1599), the National Science Foundation (DMR-1721512 and CBET-1706968), and the Donors of the American Chemical Society Petroleum Research Fund (56715-ND9).

References

- 1 H. Ohno and K. Ito, Chem. Lett., 1998, 751-752.
- 2 H. Ohno, Electrochim. Acta, 2001, 46, 1407-1411.
- 3 J. Tarascon, Nature, 2001, 414, 359-367.
- 4 J. Song, Y. Wang and C. Wan, J. Power Sources, 1999, 77, 183-197.
- 5 M. Marcinek, J. Syzdek, M. Marczewski, M. Piszcz, L. Niedzicki, M. Kalita, A. Plewa-Marczewska, A. Bitner, P. Wieczorek, T. Trzeciak, M. Kasprzyk, P. Lezak, Z. Zukowska, A. Zalewska and W. Wieczorek, Solid State Ionics, 2015, 276, 107-126.
- 6 H. Ohno, Bull. Chem. Soc. Jpn., 2006, 79, 1665-1680.
- 7 F. Fan, Y. Wang, T. Hong, M. F. Heres, T. Saito and A. P. Sokolov, Macromolecules, 2015, 48, 4461-4470.
- 8 U. H. Choi, Y. Ye, D. Salas De La Cruz, W. Liu, K. I. Winey, Y. A. Elabd, J. Runt and R. H. Colby, Macromolecules, 2014, 47, 777-790.
- 9 H. Chen, J.-H. Choi, D. Salas-dela Cruz, K. I. Winey and Y. A. Elabd, Macromolecules, 2009, 42, 4809-4816.
- 10 M. Armand, F. Endres, D. R. MacFarlane, H. Ohno and B. Scrosati, Nat. Mater., 2009, 8, 621-629.
- 11 M. Watanabe, Y. Suzuki and A. Nishimoto, Electrochim. Acta, 2000, 45, 1187-1192.
- 12 Y. Lin, J. Li, Y. Lai, C. Yuan, Y. Cheng and J. Liu, RSC Adv., 2013, 3, 10722.
- 13 R. C. Agrawal and G. P. Pandey, J. Phys. D: Appl. Phys., 2008, 41, 223001.
- 14 A. M. Christie, S. J. Lilley, E. Staunton, Y. Andreev and P. G. Bruce, Nature, 2005, 433, 50-53.
- 15 G. Jaffé and J. A. Rider, J. Chem. Phys., 1952, 20, 1071–1077.
- 16 J. R. Macdonald, Phys. Rev., 1953, 92, 4-17.
- 17 J. R. Macdonald, J. Chem. Phys., 1974, 61, 3977-3996.
- 18 R. J. Klein, S. Zhang, S. Dou, B. H. Jones, R. H. Colby and J. Runt, J. Chem. Phys., 2006, 124, 144903.
- 19 K.-J. Lin, K. Li and J. K. Maranas, RSC Adv., 2013, 3, 1564-1571.
- 20 X. G. Sun, C. L. Reeder and J. B. Kerr, Macromolecules, 2004, 37, 2219-2227.
- 21 H. Markusson, H. Tokuda, M. Watanabe, P. Johansson and P. Jacobsson, Polymer, 2004, 45, 9057-9065.
- 22 K. Lu, J. F. Rudzinski, W. G. Noid, S. T. Milner and J. K. Maranas, Soft Matter, 2014, 10, 978-989.
- 23 G. B. Appetecchi, G. T. Kim, M. Montanino, M. Carewska, R. Marcilla, D. Mecerreyes and I. De Meatza, J. Power Sources, 2010, 195, 3668-3675.

- 24 Y. Ye and Y. A. Elabd, Polymer, 2011, 52, 1309-1317.
- 25 A. Triolo, O. Russina, H.-J. Bleif and E. D. Cola, *J. Phys. Chem. B*, 2007, **111**, 4641–4644.
- 26 D. Salas-de-laCruz, M. D. Green, Y. Ye, Y. A. Elabd, T. E. Long and K. I. Winey, *J. Polym. Sci., Part B: Polym. Phys.*, 2012, 50, 338–346.
- 27 A. E. Bradley, C. Hardacre, J. D. Holbrey, S. Johnston, S. E. J. McMath and M. Nieuwenhuyzent, *Chem. Mater.*, 2002, 14, 629–635.
- 28 S. M. Urahata and M. C. C. Ribeiro, *J. Chem. Phys.*, 2005, **122**, 1–10.
- 29 M. Lee, U. H. Choi, R. H. Colby and H. W. Gibson, *Chem. Mater.*, 2010, 22, 5814–5822.
- 30 M. Lee, U. H. Choi, D. Salas-De La Cruz, A. Mittal, K. I. Winey, R. H. Colby and H. W. Gibson, *Adv. Funct. Mater.*, 2011, 21, 708–717.
- 31 U. H. Choi, M. Lee, S. Wang, W. Liu, K. I. Winey, H. W. Gibson and R. H. Colby, *Macromolecules*, 2012, 45, 3974–3985.
- 32 S. Neyertz and D. Brown, J. Chem. Phys., 1996, 104, 3797.
- 33 O. Borodin and G. D. Smith, *Macromolecules*, 1998, 31, 8396–8406.
- 34 O. Borodin and G. D. Smith, *Macromolecules*, 2000, 33, 2273–2283.
- 35 G. Mao, R. F. Perea, W. S. Howells, D. L. Price and M.-L. Saboungi, *Nature*, 2000, **405**, 163–165.
- 36 G. Mao, M.-l. Saboungi and D. L. Price, *Macromolecules*, 2002, 35, 415–419.
- 37 O. Borodin and G. D. Smith, *Macromolecules*, 2006, 39, 1620–1629.
- 38 C. Do, P. Lunkenheimer, D. Diddens, M. Gotz, M. Weib, A. Loidl, X. G. Sun, J. Allgaier and M. Ohl, *Phys. Rev. Lett.*, 2013, 111, 1–5.
- 39 J. Sangoro, C. Iacob, A. Serghei, S. Naumov, P. Galvosas, J. Kärger, C. Wespe, F. Bordusa, A. Stoppa, J. Hunger, R. Buchner and F. Kremer, J. Chem. Phys., 2008, 128, 214509.
- 40 J. R. Sangoro, C. Iacob, A. Serghei, C. Friedrich and F. Kremer, *Phys. Chem. Chem. Phys.*, 2009, **11**, 913–916.
- 41 Y. Zhang and E. J. Maginn, *J. Phys. Chem. Lett.*, 2015, **705**, 700–705.
- 42 Z. Wojnarowska, J. Knapik, M. Díaz, A. Ortiz, I. Ortiz and M. Paluch, *Macromolecules*, 2014, 47, 4056–4065.
- 43 J. R. Sangoro, C. Iacob, A. L. Agapov, Y. Wang, S. Berdzinski, H. Rexhausen, V. Strehmel, C. Friedrich, A. P. Sokolov and F. Kremer, *Soft Matter*, 2014, **10**, 3536–3540.
- 44 F. Fan, W. Wang, A. P. Holt, H. Feng, D. Uhrig, X. Lu, T. Hong, Y. Wang, N. G. Kang, J. Mays and A. P. Sokolov, *Macromolecules*, 2016, **49**, 4557–4570.
- 45 S. Mogurampelly, J. Keith and V. Ganesan, *J. Am. Chem. Soc.*, 2017, **139**, 9511–9514.
- 46 G. Chevrot, R. Schurhammer and G. Wipff, *Phys. Chem. Chem. Phys.*, 2006, **8**, 4166–4174.
- 47 T. I. Morrow and E. J. Maginn, *J. Phys. Chem. B*, 2002, **106**, 12807–12813.
- 48 M. G. D. Pópolo and G. A. Voth, *J. Phys. Chem. B*, 2004, **108**, 1744–1752.
- 49 C. J. Margulis, Mol. Phys., 2004, 102, 829-838.

- 50 J. N. A. C. Lopes and A. A. H. Pádua, J. Phys. Chem. B, 2006, 110, 3330–3335.
- 51 Y. Wang and G. A. Voth, *J. Am. Chem. Soc.*, 2005, **127**, 12192–12193.
- 52 Y. Wang and G. A. Voth, *J. Phys. Chem. B*, 2006, **110**, 18601–18608.
- 53 S. Plimpton, J. Comput. Phys., 1995, 117, 1-19.
- 54 W. L. Jorgensen, D. S. Maxwell and J. Tirado-Rives, J. Am. Chem. Soc., 1996, 118, 11225–11236.
- 55 S. V. Sambasivarao and O. Acevedo, J. Chem. Theory Comput., 2009, 5, 1038–1050.
- 56 B. L. Bhargava and S. Balasubramanian, *J. Chem. Phys.*, 2007, 127, 114510.
- 57 J. M. Wang, R. M. Wolf, J. W. Caldwell, P. A. Kollman and D. A. Case, J. Comput. Chem., 2004, 25, 1157–1174.
- 58 J. Wang, W. Wang, P. A. Kollman and D. A. Case, J. Mol. Graphics Modell., 2006, 25, 247–260.
- 59 M. Frisch, G. Trucks, H. Schlegel, G. Scuseria, M. Robb, J. Cheeseman, G. Scalmani, V. Barone, B. Mennucci and G. Peterson, *Gaussian 09*, 2009.
- 60 J. N. Canongia Lopes, J. Deschamps and A. A. H. Pádua, J. Phys. Chem. B, 2004, 108, 16893–16898.
- 61 F. Dommert, K. Wendler, R. Berger, L. Delle Site and C. Holm, *ChemPhysChem*, 2012, 13, 1625–1637.
- 62 J. Mondal, E. Choi and A. Yethiraj, *Macromolecules*, 2013, 47, 438–446.
- 63 O. Borodin, G. D. Smith and W. Henderson, *J. Phys. Chem. B*, 2006, **110**, 16879–16886.
- 64 O. Borodin, J. Phys. Chem. B, 2009, 113, 11463-11478.
- 65 O. Borodin, W. Gorecki, G. D. Smith and M. Armand, *J. Phys. Chem. B*, 2010, **114**, 6786–6798.
- 66 C. Y. Son, J. G. McDaniel, J. R. Schmidt, Q. Cui and A. Yethiraj, J. Phys. Chem. B, 2016, 120, 3560–3568.
- 67 J. G. McDaniel, E. Choi, C.-Y. Son, J. R. Schmidt and A. Yethiraj, J. Phys. Chem. B, 2016, 120, 231–243.
- 68 Y. Zhang, L. Xue, F. Khabaz, R. Doerfler, E. L. Quitevis, R. Khare and E. J. Maginn, *J. Phys. Chem. B*, 2015, **119**, 14934–14944.
- 69 T. G. A. Youngs and C. Hardacre, *ChemPhysChem*, 2008, 9, 1548–1558.
- 70 V. Chaban, Phys. Chem. Chem. Phys., 2011, 13, 16055-16062.
- 71 V. V. Chaban, I. V. Voroshylova and O. N. Kalugin, *Phys. Chem. Chem. Phys.*, 2011, 13, 7910–7920.
- 72 Y. Zhang and E. J. Maginn, *J. Phys. Chem. B*, 2012, **116**, 10036–10048.
- 73 A. Mondal and S. Balasubramanian, *J. Phys. Chem. B*, 2014, **118**, 3409–3422.
- 74 A. P. Sunda, A. Mondal and S. Balasubramanian, *Phys. Chem. Chem. Phys.*, 2015, **17**, 4625–4633.
- 75 R. Hockney and J. Eastwood, *Computer Simulation Using Particles*, CRC Press, 1988.
- 76 S. Plimpton, R. Pollock and M. J. Stevens, Proceedings of the Eighth Siam Conference on Parallel Processing for Scientific Computing, 1997, pp. 1–13.
- 77 W. Shinoda, M. Shiga and M. Mikami, Phys. Rev. B: Condens. Matter Mater. Phys., 2004, 69, 134103.

- 78 G. J. Martyna, D. J. Tobias and M. L. Klein, *J. Chem. Phys.*, 1994, **101**, 4177–4189.
- 79 M. Parrinello and A. Rahman, *J. Appl. Phys.*, 1981, 52, 7182–7190.
- 80 M. E. Tuckerman, J. Alejandre, R. López-Rendón, A. L. Jochim and G. J. Martyna, *J. Phys. A: Math. Gen.*, 2006, **39**, 5629–5651.
- 81 J. P. Ryckaert, G. Ciccotti and H. J. C. Berendsen, *J. Comput. Phys.*, 1977, **23**, 327–341.
- 82 T. Schneider and E. Stoll, *Phys. Rev. B: Condens. Matter Mater. Phys.*, 1978, **17**, 1302–1322.
- 83 L. Martinez, R. Andrade, E. Birgin and J. Martinez, *J. Comput. Chem.*, 2009, **30**, 2157–2164.

- 84 W. Zhao, F. Leroy, B. Heggen, S. Zahn, B. Kirchner, S. Balasubramanian and F. Müller-Plathe, *J. Am. Chem. Soc.*, 2009, **131**, 15825–15833.
- 85 M. G. Del Pópolo, C. L. Mullan, J. D. Holbrey, C. Hardacre and P. Ballone, *J. Am. Chem. Soc.*, 2008, **130**, 7032–7041.
- 86 A. Chandra, Phys. Rev. Lett., 2000, 85, 768-771.
- 87 T. G. Fox and P. J. Flory, J. Appl. Phys., 1950, 21, 581-591.
- 88 K. Nakamura, K. Fukao and T. Inoue, *Macromolecules*, 2012, 45, 3850–3858.
- 89 N. Shamim and G. B. McKenna, *J. Phys. Chem. B*, 2010, **114**, 15742–15752.
- 90 J. R. Keith, S. Mogurampelly, B. K. Wheatle and V. Ganesan, J. Polym. Sci., Part B: Polym. Phys., 2017, 55, 1718–1723.